THE ASTROPHYSICAL JOURNAL, 196:227–250, 1975 February 15

THE ATMOSPHERE AND IONOSPHERE OF IO

MICHAEL B. MCELROY AND YUK LING YUNG
Center for Earth and Planetary Physics, Harvard University
Received 1974 May 30; revised 1974 August 23

ABSTRACT

A variety of models for Io's atmosphere, ionosphere, surface, and environment are developed and discussed in the context of recent observational data. The sodium emission detected by Brown appears to require a collisional excitation process in Io's atmosphere, and the extended sodium emission measured by Trafton *et al.* may require scattering of the planetary radiation by an extended sodium cloud. The sodium is presumably present initially in bound form on Io's surface and may be released by the sputtering mechanism suggested by Matson *et al.* The ionosphere detected by the radio occultation experiment on *Pioneer 10* could be attributed to photoionization of atmospheric sodium if Io's atmosphere could sustain significant vertical motions, of order 1 s^{-1} directed up during the day, down at night. Vertical motions of this magnitude could be driven by condensation of atmospheric NH_3. The total density of gas at Io's surface appears to lie in the range 10^{10}–10^{12} molecules cm^{-3}. Corpuscular ionization could play an additional role for the ionosphere. In this case the satellite should exhibit an exceedingly bright, ~10 kR, airglow at Lα. The incomplete hydrogen torus observed by Judge and Carlson in the vicinity of Io requires a large supply of hydrogen from the satellite's atmosphere. The escape flux should be of order 10^{11} cm^{-2} s^{-1} and could be maintained by photolysis of atmospheric NH_3. The observed geometry of the hydrogen torus appears to require a surprisingly short lifetime, $\sim 10^5$ s, for neutral hydrogen near Io's orbit, and may indicate the presence of a large flux, $\sim 10^9$ cm^{-2} s^{-1}, of low-energy protons in Jupiter's magnetosphere. Implications of the hydrogen torus for the energy and mass balance of Jupiter's magnetosphere are discussed briefly, and observational programs are identified which might illuminate present uncertainties in our understanding of Io.

Subject headings: atmospheres, planetary — Jupiter — satellites

I. INTRODUCTION

Brown's (1973) announcement of intense radiation from Io in the D lines of atomic sodium has sparked a major revival of interest in the properties of Jupiter's innermost Galilean satellite. It is now clear that the radiation is emitted from an extended region of space around Io and that both the extent and intensity of the emission may change with time (Trafton, Parkinson, and Macy 1974; Brown and Chaffee 1974). The lines are remarkably broad, and the ratio of line intensities, D_2/D_1, is variable with values ranging from as low as 1.2 to perhaps as high as 2.3 (Brown and Chaffee 1974; Trafton *et al.* 1974).

A simple model was proposed by McElroy, Yung, and Brown (1974) to describe the gross features of the observations. Following an earlier suggestion by Sinton (1973), they assumed that Io's atmosphere contained major quantities of ammonia gas in equilibrium with a layer of surface ice. Photolysis of NH_3 could provide an important source of atmospheric nitrogen, and they argued that collisions between sodium atoms and vibrationally excited nitrogen could account for the necessary excitation of the D lines. The mechanism was similar to that thought to apply in terrestrial aurorae (Hunten 1965). In order to explain the observed values for the ratio of line intensities, D_2/D_1, McElroy *et al.* (1974) invoked an optically thick sodium atmosphere, with spatial separation between the source and scattering regimes. They assumed that the observed radiation was scattered by a cloud of sodium ejected from Io during periods of intense atmospheric heating. The required heating could be generated by an electromagnetic interaction of Io with the external Jovian magnetosphere. The ratio of line intensities should vary from a value close to 1.0 when the cloud was compact and optically thick, to a value approaching 2.0 as the cloud became diffuse and optically thin.

The behavior discussed above is in general agreement with observation. Resonance scattering of sunlight by the diffuse sodium cloud may be important, however, and was not explicitly included in the earlier model. Its role was discussed briefly by Trafton *et al.* (1974), by Matson, Johnson, and Fanale (1974), and by Parkinson (1974). Parkinson concluded that resonance scattering alone could not account for the observed range of values for the ratio of line intensities D_2/D_1, and he favored a combination of sources, resonance scattering plus internal excitation, to explain the observations. His analysis did not, however, allow for complexities introduced by multiple scattering. A more extensive discussion of the resonance scattering model is given below, in § II. As we shall see, scattering theory can be used to place an upper limit on the column density of atomic sodium in Io's quiescent atmosphere. This limit imposes important constraints on theoretical models for Io's ionosphere, and allows us to draw some further conclusions regarding the density and composition of the bulk atmosphere, as discussed in § III.

Kliore *et al.* (1974) reported the detection of a well developed ionosphere on the dayside of Io, with a peak electron density of 6×10^4 cm^{-3} at an approximate altitude of 100 km. Further work (Kliore 1974) indicates the

presence of an ionosphere also on the nightside of Io, with an electron density of order 10^4 cm^{-3} near the satellite's surface shortly before local sunrise. We shall argue that the ionosphere is most probably composed of Na^+, formed by photoionization of Na, although there may be an additional contribution due to corpuscular bombardment. The atmosphere should contain major concentrations of a hydrogen-rich, condensable, molecular gas, and NH_3 is an obvious candidate. The ionospheric theory allows us to determine a value for the product of the concentrations of neutral sodium and total gas. This result, coupled with the upper limit for sodium derived from the airglow analysis, allows us to place a lower bound on the total atmospheric density. We show also that the temperature derived from analysis of the ionospheric data is consistent with the result expected from a detailed study of the atmospheric energy budget.

Further clues to the processes which regulate conditions in Io's atmosphere can be derived from an analysis of the airglow measurements carried out by Judge and Carlson (1974) with instrumentation on *Pioneer 10*. They detected a bright ultraviolet glow from the vicinity of Io. If the glow is predominantly due to Lα emission, as seems probable, their observations would indicate an intensity of approximately 300 R. The emission appears to precede and follow Io along its orbit. It has a spatial extent in the orbital plane of approximately 120° and a vertical extent of less than one Jovian diameter. The analysis indicates a lifetime for atomic hydrogen of order 10^5 s and suggests a high flux, $\sim 10^9$ cm^{-2} s^{-1}, for the low-energy proton component of Jupiter's trapped radiation. Charge transfer with fast protons could be an important sink for hydrogen, and we discuss some implications of this reaction for the mass and energy balance of the magnetosphere. An escape flux of hydrogen, from Io, of order 10^{11} cm^{-2} s^{-1} is required to supply the extensive hydrogen cloud. We discuss the implications of this result for Io's atmosphere and note that the flux could be readily supplied by photolysis of NH_3.

The composition of Io's surface material remains undefined. Ammonia ice, either in the pure form or as a hydrate, remains an attractive possibility. The presence of significant concentrations of dissolved sodium in the NH_3 ice could make the ice electrically conductive and mask the characteristic infrared absorption features which might be expected for the pure ice form. Other possibilities for the surface layer include $NaNH_2$ formed photochemically in the atmosphere, and a variety of salt deposits rich in sulfur and sodium as suggested by Fanale, Johnson, and Matson (1974). Sputtering, induced by the impact of energetic particles on the surface, appears to be the most plausible mechanism for release of bound sodium (Matson *et al.* 1974). The magnitude of the sodium source is uncertain, however. A flux of order 2×10^7 atoms cm^{-2} s^{-1} would be required to supply the extended sodium cloud if resonance scattering of sunlight were the predominant excitation mechanism for the observed radiation. Smaller fluxes could be accommodated if the glow were produced by scattering of radiation excited by collisional processes in Io's atmosphere.

We offer brief comments on future observational programs which might resolve present ambiguities. A search for a possible correlation of Io's optical activity with Jupiter's decametric activity would be particularly valuable. A search for the possible presence of emissions associated with N_2^+, N, H, and Ca would also be useful, and high-resolution spectra of the satellite at infrared wavelengths could narrow the range of speculation regarding the surface composition. There is a need for further observations at ultraviolet wavelengths, and we expect that these data could be obtained with a suitably designed experiment on the Mariner mission scheduled for launch in 1977.

II. MODELS FOR SODIUM EMISSION

We discuss here three possible models for the observed sodium airglow. The models are shown schematically in figure 1. Models A and B assume that the sodium radiation is excited primarily by collisional processes in the atmosphere. Resonance scattering of incident sunlight is the dominant excitation mechanism in model C. Models A and B allow for spatial separation between the radiation source and scattering regions. The source is placed below the scattering layer in model A, above in model B.

The collisional source is assumed to populate excited states of sodium at rates proportional to their statistical weight. Thus, primary excitation rates for D_2 exceed those for D_1 by a factor of 2.0 in models A and B. The corresponding value for model C is 1.7, reflecting factors of 0.85 and 2.0 in the incident solar fluxes and oscillator strengths, respectively. The ratio of excitation rates remains relatively constant in model C, as Io moves around its orbit, although the rates for excitation of the individual lines vary by as much as a factor of 10 due to Doppler shift of the incident sunlight (Parkinson 1974).

The intensity of radiation at wavelength λ in the D lines is given by solution of an appropriate transfer equation. Assuming plane-parallel geometry, and using standard notation, we have

$$\mu \frac{dI_\lambda}{d\tau} = I_\lambda - \frac{1}{2}\int_{-1}^{1} I_\lambda d\mu - \epsilon , \tag{1}$$

where ϵ defines the strength of the primary radiation source. In models A and B we set ϵ equal to a constant in the source region, equal to zero elsewhere. For model C,

$$\epsilon = \tfrac{1}{4} F_\lambda \exp\left[-\frac{\tau(\lambda)}{\mu_0}\right], \tag{2}$$

where πF_λ defines the flux of incident sunlight.

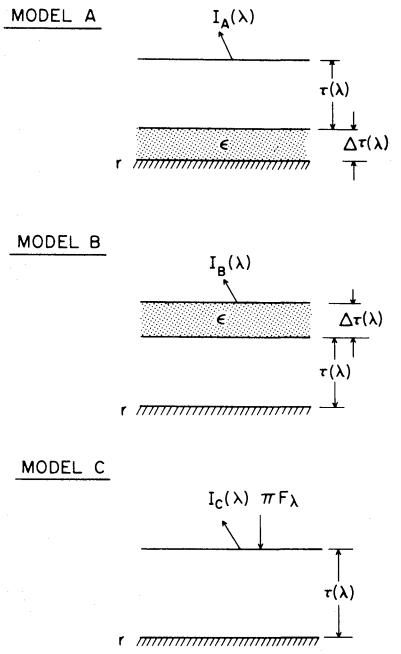

FIG. 1.—Schematic diagrams for sodium emission illustrating the assumptions for models A, B, and C

The thickness of the scattering layer in models A and B is given by

$$\tau(\lambda) = \tau_0 \exp\left[-\left(\frac{\lambda - \lambda_0}{\Delta\lambda}\right)^2\right]. \tag{3}$$

The thickness of the source region is specified by

$$\Delta\tau(\lambda) = \Delta\tau_0 \exp\left[-\rho^2\left(\frac{\lambda - \lambda_0}{\Delta\lambda}\right)^2\right], \tag{4}$$

where

$$\rho = (T_1/T_2)^{1/2} \tag{5}$$

and

$$\Delta\lambda = \frac{\lambda_0}{c}(2kT_1/M)^{1/2}. \tag{6}$$

Here T_1 and T_2 are the temperatures of the scattering and source regions, respectively.

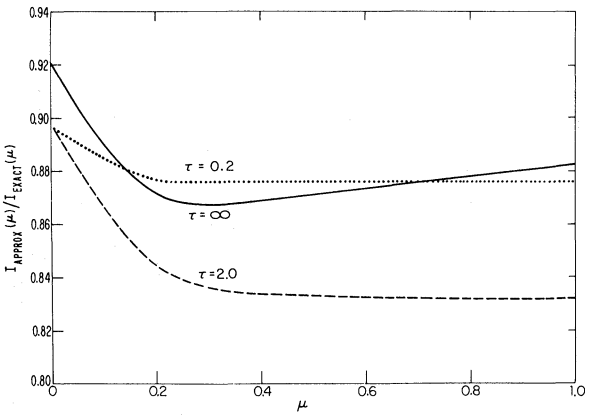

FIG. 2.—Ratio, $I_{approx}(\mu)$ $I_{exact}(\mu)$, of approximate to exact intensities versus μ, the cosine of the zenith angle. $I_{approx}(\mu)$ is calculated using the two-stream approximation. $I_{exact}(\mu)$ is calculated using tabulated values of X, Y, and H functions. The cosine of the angle of incident sunlight μ_0 is taken to be 1.

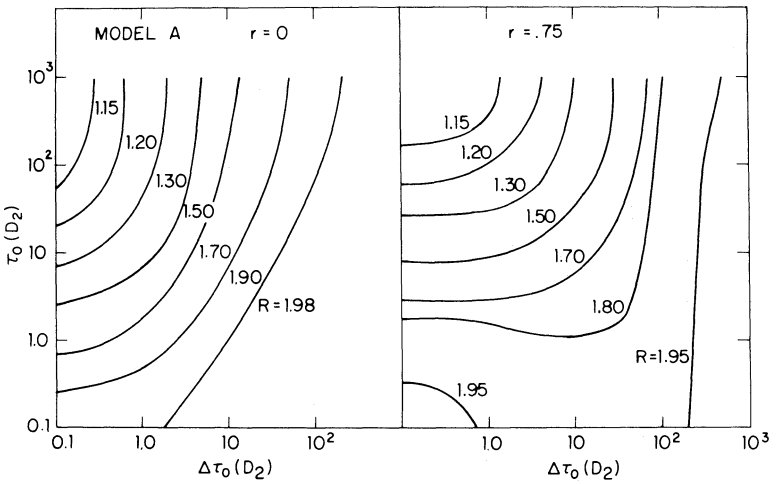

FIG. 3.—Ratio R of emergent D_2 to D_1 intensities computed with model A. The values of $\Delta\tau_0(D_2)$ and $\tau_0(D_2)$ range from 0.1 to 10^3. Results are presented for surface reflectivities $r = 0$ and $r = 0.75$. In this and subsequent figures T_1 is set equal to T_2.

The intensity of radiation emerging at wavelength λ in the D_1 line can be readily calculated using a two-stream approximation to solve equation (1). This procedure is justified for present purposes: we verified that the associated errors are typically less than 20 percent, as shown schematically for model C in figure 2. The intensity of radiation emitted at a zenith angle θ such that $\mu = \cos\theta = 1/\sqrt{3}$ is given by

$$I^{D_1}{}_A(\lambda) = \frac{3^{1/2}\epsilon\Delta\tau(\lambda)[2(1+r) + (1-r)3^{1/2}\Delta\tau(\lambda)]}{2 + (1-r)3^{1/2}[\Delta\tau(\lambda) + \tau(\lambda)]}, \tag{7}$$

$$I^{D_1}{}_B(\lambda) = \frac{3^{1/2}\epsilon\Delta\tau(\lambda)\{2(1+r) + (1-r)3^{1/2}[2\tau(\lambda) + \Delta\tau(\lambda)]\}}{2 + (1-r)3^{1/2}[\Delta\tau(\lambda) + \tau(\lambda)]}, \tag{8}$$

and

$$I^{D_1}{}_C(\lambda) = \frac{3^{1/2}}{2}\frac{F_\lambda[[2 - (1+r)e^{-\tau(\lambda)} + (1-r)\{3^{1/2}[e^{-\tau(\lambda)} + \tau(\lambda) - 1] - 1\}]]}{2 + (1-r)3^{1/2}\tau(\lambda)} \tag{9}$$

for models A, B, and C respectively. Results for other values of θ can be readily calculated using relations given in the Appendix. We assumed that the surface albedo r was independent of λ. The intensity of the D_2 line is simply obtained from relations (7)–(9) by doubling the appropriate values of $\Delta\tau$ and τ, and using the approximate relation

$$F_\lambda(D_1) = 1.18F_\lambda(D_2). \tag{10}$$

The important observational quantities are the ratio of emergent line intensities D_2/D_1, the width of the individual lines, and their intensity. The line intensity ratio is given by

$$R = \frac{\int I^{D_2}(\lambda)d\lambda}{\int I^{D_1}(\lambda)d\lambda}, \tag{11}$$

and other observable quantities may be readily computed using equations (2)–(10).

Values of R are given in figure 3 for model A. Results are shown for two values of the surface reflectivity, $r = 0.75$ and $r = 0$. As may be readily demonstrated, the ratio of line intensities tends to the optically thin limit, $R = 2.0$, for all values of $\Delta\tau_0$ and τ_0 as $r \to 1.0$. The results with $r = 0.75$ model the case in which Io's surface represents an important sink for backscattered radiation. The results with $r = 0$ would be appropriate if both the source and scattering regions were detached from the planet, such that surface reflectance played a negligible role.

Values of R obtained with model A range between 1.0 and 2.0, with the smaller values appropriate for large optical thickness in the scattering layer. Scattering is more important for the stronger line, D_2. This radiation is preferentially trapped in the lower atmosphere, and is selectively absorbed by the planetary surface, or by black space, with consequent reduction in the computed ratio of emergent line intensities. The ratio R is an increasing function of $\Delta\tau_0$ for fixed values of τ_0, reflecting the change in the relative positions of the upper and lower boundaries with respect to the radiation source region.

Profiles of the emergent D_2 line, computed with model A, are shown in figure 4 for $\Delta\tau_0 = 0.5$ and for various values of τ_0. As is evident in the figure, scattering leads to significant broadening of the emergent line. The broadening occurs due to selective absorption of radiation near the line center, and, as discussed by McElroy *et al.* (1974),

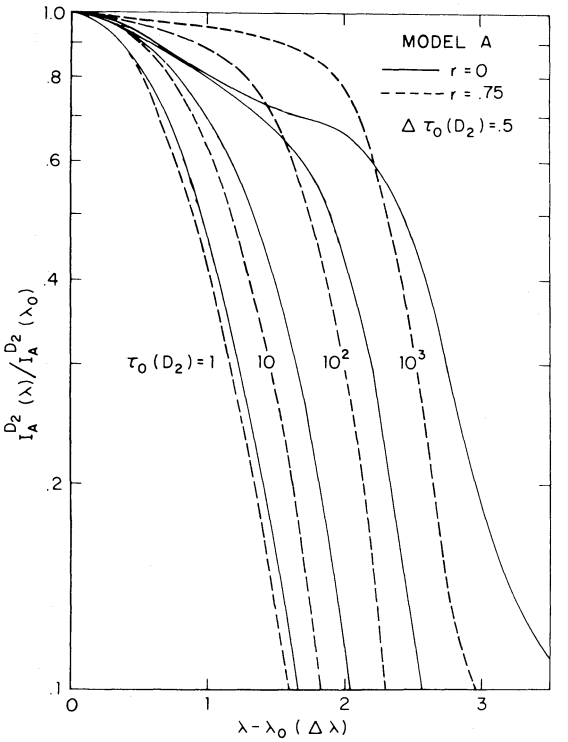

FIG. 4.—Profiles of the emergent D_2 line computed with model A for $\Delta\tau_0(D_2) = 0.5$ and $\tau_0(D_2) = 1, 10, 10^2, 10^3$. Profiles are normalized to given unit intensity at the line center. Wavelength λ is measured in units of Doppler width $\Delta\lambda$. Results are presented for surface reflectivities $r = 0$ (*solid line*) and $r = 0.75$ (*dashed line*).

this mechanism may provide a simple explanation for the broad line observed by Brown and Chaffee (1974). If we adopt the upper limit for $\tau_0 + \Delta\tau_0$ derived below, it should be possible to account for the observed profile with an emission temperature as low as 5000° K. A comparable temperature would be required with model C, but a higher temperature, ~50,000° K, would be required for model B.

Values of R obtained with model B are shown in figure 5, and corresponding profiles for the emergent D_2 line are given in figure 6. The ratio of emergent line intensities is larger than 2.0 for all cases in which $\tau_0 > 3\Delta\tau_0$. Maximum values of R are predicted for the computations with $r = 0$. The increase in R over its optically thin limit occurs due to selective absorption of D_1 at the planetary surface. The optical depth in the scattering layer is less for D_1 than

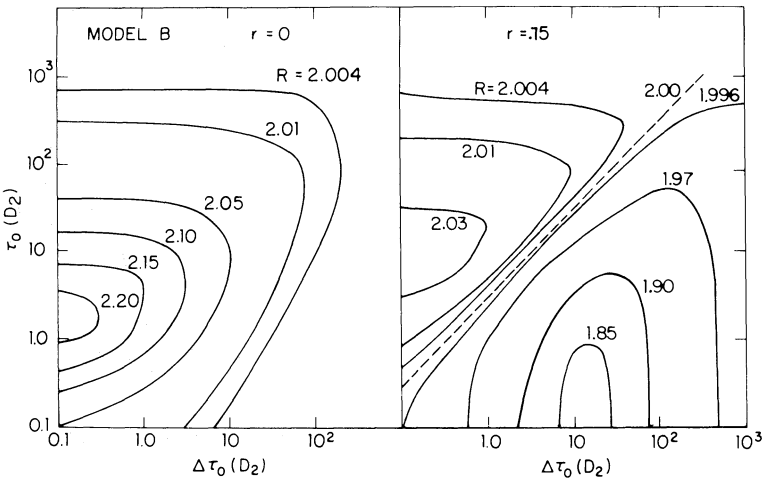

FIG. 5.—Ratio R of emergent D_2 to D_1 intensities computed with model B. The values of $\Delta\tau_0(D_2)$ and $\tau_0(D_2)$ range from 0.1 to 10^3. Results are presented for surface reflectivities $r = 0$ and $r = 0.75$.

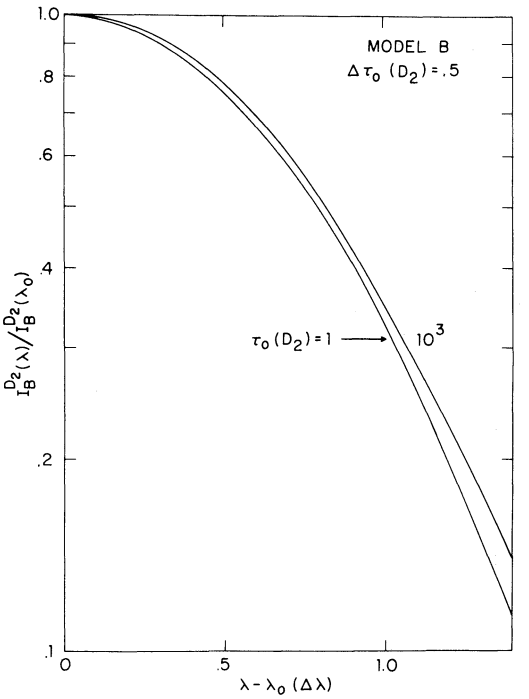

FIG. 6.—Profiles of the emergent D_2 line computed with model B for $\Delta\tau_0(D_2) = 0.5$ and $\tau_0(D_2) = 1, 10^3$. Profiles are normalized to give unit intensity at the line center. Wavelength λ is measured in units of Doppler width $\Delta\lambda$. Results are presented for surface reflectivity $r = 0$. Results for $r = 0.75$ are essentially identical.

for D_2. As a consequence, radiation in the D_1 line can be transmitted more efficiently from the source region to the surface sink. As illustrated in figure 6, radiative transfer leads to trivial broadening of the emergent lines in model B, in contrast to the behavior indicated for model A.

Results for model C are summarized in figures 7–9. In the limit of small optical thickness the intensity is proportional to τ_0, and the ratio of emergent line intensities approaches the limiting value $R = 1.7$. For moderately

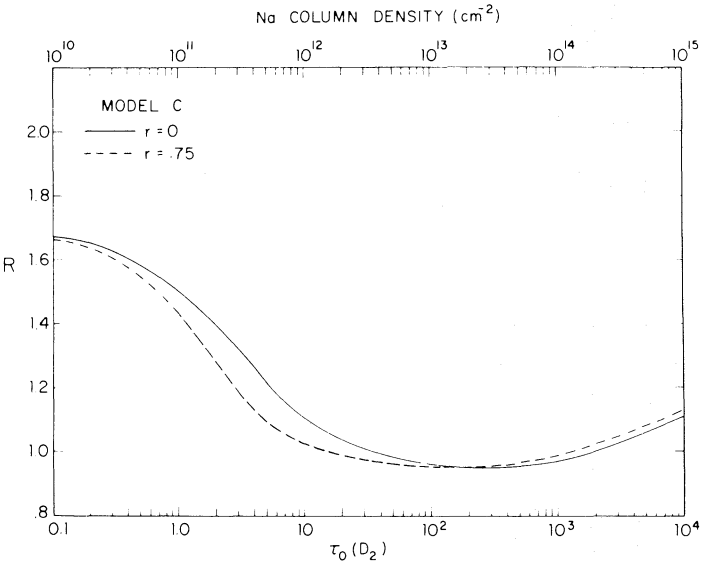

FIG. 7.—Ratio R of emergent D_2 to D_1 intensities computed with model C. Ratio, $\pi F_\lambda(D_2)/\pi F_\lambda(D_1)$, of incident solar fluxes is taken to be 0.85. Results are presented for surface reflectivities $r = 0$ (*solid line*) and $r = 0.75$ (*dashed line*).

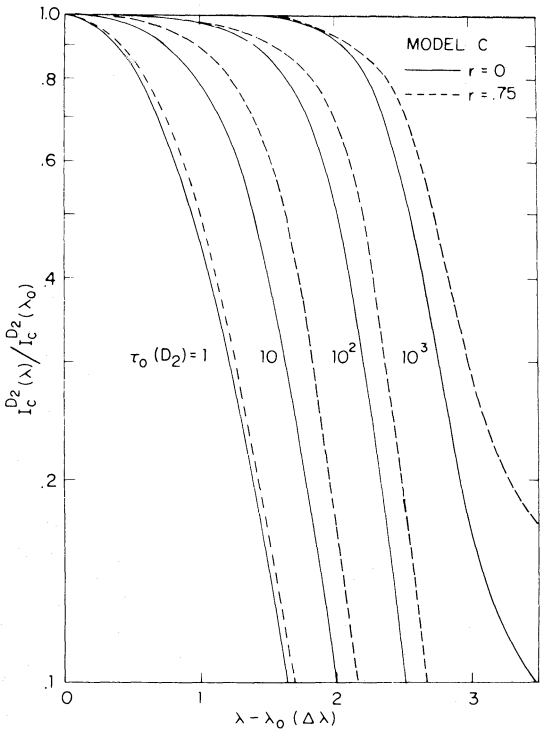

FIG. 8.—Profiles of the emergent D_2 line computed with model C for $\Delta\tau_0(D_2) = 0.5$ and $\tau_0(D_2) = 1, 10, 10^2, 10^3$. Profiles are normalized to give unit intensity at the line center. Wavelength λ is measured in units of Doppler width $\Delta\lambda$. Results are presented for surface reflectivities $r = 0$ (*solid line*) and $r = 0.75$ (*dashed line*).

large values of τ_0, of order 10^2, the Doppler core is strongly saturated and the emergent intensity varies as $(\log \tau_0)^{1/2}$. The intensity ratio in this case is given by

$$R \simeq 0.85\left[\frac{\log \tau_0}{\log (\tau_0/2)}\right]^{1/2} \simeq 0.85\left(1 + \frac{1}{2}\frac{\log 2}{\log \tau_0}\right). \tag{12}$$

At still larger values of τ_0, the intensity of the emergent radiation is determined primarily by scattering in the natural wings of the atomic lines, and the emergent intensity varies as $\tau_0^{1/2}$, such that $R \to 1.2$. Radiative transfer

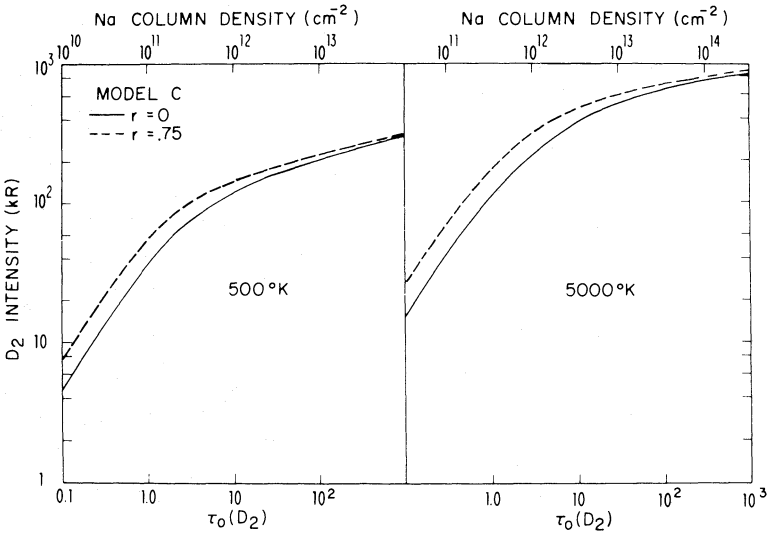

FIG. 9.—Intensity of sodium D_2 emission versus sodium abundance expressed in terms of optical depth and total column density. The solar flux is taken as 1.2×10^{12} photons $cm^{-2}\,s^{-1}\,Å^{-1}$. Results are presented for surface reflectivities $r = 0$ (*solid line*) and $r = 0.75$ (*dashed line*) and for temperatures 500° and 5000° K.

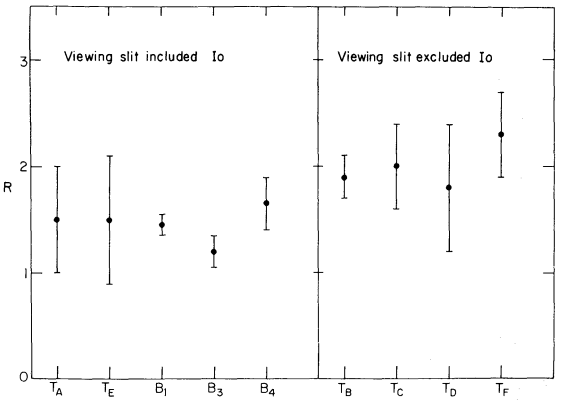

FIG. 10.—D_2 to D_1 intensity ratio, R, as measured by Trafton *et al.* (1974) (T_A, T_B, T_C, T_D, T_E, T_F), and by Brown *et al.* (1974) (B_1, B_2, B_3, B_4). We distinguish between measurements of R taken with Io in the viewing slit and those taken with Io excluded from the field of view.

leads to major broadening of the spectral lines predicted by model C, as shown in figure 8. The profiles predicted with model C are significantly broader than profiles calculated with model B, but comparable to those derived with model A. Profiles computed with the various models exhibit characteristically different behavior for frequencies near the line center, offering the possibility for future observational discrimination between the models.

The intensity of the emergent D_2 line, predicted on the basis of model C, is shown in figure 9. We assumed an incident solar flux of 1.2×10^{12} photons $cm^{-2}\ s^{-1}\ Å^{-1}$, and the results given here apply therefore during times when Io is at maximum elongation with respect to the Sun (Trafton *et al.* 1974). The intensity is less at other times and should be reduced by approximately a factor of 10 in order to model conditions near inferior and superior conjunction, when the Doppler shift of the incident sunlight has its smallest value.

We can readily derive an upper limit for the column density of atomic sodium in Io's atmosphere, using the results given in figure 9. Brown and Chaffee (1974) found no evidence for sodium emission in a spectrum of Io taken on 1973 October 5 when the Sun–Jupiter–Io angle had a value of 43°. Io occupied between one-third and one-quarter of the field of view during the observing period, and the results can be interpreted to set an upper limit of between 60 kR and 80 kR for the intensity of the D_2 line emitted by Io. If we reduce the intensity scale in figure 9 by a factor of 2 to allow for the appropriate Doppler shift of the incident solar radiation, and assume a temperature of 500° K for the quiescent atmosphere, in accord with the discussion below, we find that $\tau_0(D_2)$ must be less than 100. The observation implies, therefore, an upper limit for the column concentration of sodium of about 10^{13} atoms cm^{-2}. We shall assume that this limit applied also at the time when Io's ionosphere was probed by the radio signal from *Pioneer 10*; and, as we shall see, the limit imposes serious constraints on theoretical models for the ionosphere.

Observations of the extended sodium emission around Io can be used to derive some useful information on the magnitude of the atomic source at Io's surface which would be required to supply the radiating cloud. We shall assume that the lifetime of a sodium atom in Io's environment is set by the time required for photoionization, approximately 3 weeks.[1] Ionization represents a net sink for gas in the cloud since atoms will be swept up and carried away by Jupiter's magnetic field after they are ionized. We shall assume that the intensity of the D-line emission from the sodium cloud is determined primarily by resonance scattering of incident sunlight. The analysis should therefore provide an upper bound for the magnitude of the necessary sodium source strength. Using the results reported by Trafton *et al.* (1974), which imply an average intensity of 15 kR for D_2 emission and an approximate radius of 10^5 km for the emitting cloud, we estimate a surface source of 2×10^7 atoms $cm^{-2}\ s^{-1}$. The actual source strength could be significantly less than this result. The analysis given here depends critically on the assumption that resonance scattering of sunlight should be the dominant mechanism for excitation of the observed sodium radiation.

Figure 10 gives a summary of line intensity ratios R measured by various observers. We distinguish between observations taken with Io in the field of view and those for which Io was excluded. There appears to be a significant difference in the values of R obtained for the separate viewing geometries. An average of all observations including Io yields an intensity ratio R equal to 1.45 ± 0.20. The corresponding analysis with Io excluded from the field of view gives R equal to 2.00 ± 0.28, and suggests that resonance scattering of sunlight may not be the major excitation process in the extended cloud. Both results are consistent with model A, or with a combination of models A and B. They can be explained by an internal excitation mechanism such as that suggested by McElroy

[1] Charge transfer with trapped magnetospheric ions could offer an additional sink for sodium. Lack of observational data on the density of low-energy trapped radiation precludes any quantitative estimate of its effect. As discussed later, however, we consider it unlikely that charge transfer should play a major role for sodium, although it may dominate as a sink for hydrogen.

et al. (1974), with the emergent radiation scattered by a cloud of sodium ejected by Io. As the cloud expands, it becomes optically thin, and the intensity ratio tends to 2.0 as indicated in figure 3. Further observations, either to confirm or deny the trend suggested by figure 10, would be instructive and should shed valuable light on the nature of the sodium excitation mechanism. Simultaneous observations of Io and its immediate neighborhood, with suitable spatial resolution, would be especially useful.

III. MODELS FOR THE IONOSPHERE

The electron density n satisfies the usual continuity equation

$$\frac{\partial n}{\partial t} + \nabla\cdot(n\boldsymbol{v}) = P - L\,, \tag{13}$$

where P and L are the volume production and loss rates, respectively. We shall assume that variations of n and $\boldsymbol{v}$ with horizontal coordinates are small compared with the corresponding variation with the vertical coordinate z. Then equation (13) may be rewritten in the form

$$\frac{\partial n}{\partial t} + \frac{\partial}{\partial z}(nw) = P - L\,, \tag{14}$$

where w is the vertical velocity, given by

$$w = w_0 + w_d\,. \tag{15}$$

The quantity w_0 defines the bulk vertical motion of the background neutral atmosphere, and w_d is an appropriate diffusion velocity.

The diffusion velocity is given by

$$w_d = -\frac{D}{n}\left(\frac{\partial n}{\partial z} + \frac{n}{H}\right), \tag{16}$$

where D is the diffusion coefficient and H is the equilibrium value for the electron scale height. If the composition of the ionosphere is dominated by a single species of positive ion, i, such that $n \simeq n_i$, then

$$H = 2kT/M_i g\,, \tag{17}$$

where M_i is the mass of the predominant positive ion. The expression for H is more complex if several ionic species contribute significantly to the observed electron density (cf. Bates and Patterson 1962).

We investigated a number of possible models for Io's ionosphere. The models were generated by numerical solution of equations (14)–(16). An acceptable model must satisfy several restrictive, and to some extent contradictory, conditions. It must account for the surprisingly high value observed for the electron concentration on the dayside of the planet. At the same time the model must allow for rapid decay of ionization on the nightside in order to provide consistency with the ionospheric results derived from analysis of the occultation data obtained during egress. Electron densities observed on the dayside showed a peak concentration of 6×10^4 cm^{-3} at an altitude of 100 km. In contrast, the maximum concentration at night was about 10^4 cm^{-3}, and the peak occurred close to the planetary surface. The scale height above the peak on the dayside was about 200 km. The nightside scale height appeared to be significantly less than this value (Kliore *et al.* 1974).

We shall focus attention mainly on models in which electrons are formed by photoionization of atmospheric gases. Photoionization of NH_3 dominates for model 1. Photoionization of Na is the major ionization source in models 2 through 5, and possible effects of corpuscular ionization are considered in model 6. Vertical motion of the background atmosphere plays an important role in model 4, tending to raise the level of the ionization maximum during the day and to lower it at night in accord with observation. The vertical velocity w_0 is set equal to zero in models 1, 2, 3, 5, and 6. Detailed assumptions of the various models are summarized in table 1.

The results for model 1 are displayed in figure 11. We show here computations for the daytime ionosphere. Dissociative recombination provides the major sink for ionization. The associated rate constant is large, $\sim 10^{-7}$ cm^3 s^{-1}, and as a consequence the ionosphere decays rapidly at night, in accord with observation. Model 1 fails, however, to account for the observed magnitude of the electron density at the ionization maximum in the daytime ionosphere. This feature of the results is characteristic of all photoionization models in which molecular species dominate. Under these conditions ionization rates are too slow, and recombination rates too fast, to account for the observed daytime concentration of electrons. We may note that the density of electrons at Io's ionospheric maximum is comparable to the density of electrons observed at similar levels in the atmospheres of Mars and Venus (Kliore *et al.* 1965; Kliore *et al.* 1967), although the available flux of ionizing solar radiation is significantly less, by factors of 12 and 52, respectively.

TABLE 1

MODELS FOR THE IONOSPHERE OF Io

Model*	Atmospheric Composition† (cm^{-3})	Atmospheric Temperature (° K)	Vertical Velocity ($cm\ s^{-1}$)	Major Ion	Electron Source‡	Electron Loss
1.....	$NH_3 = 10^9, 10^{10}, 10^{11}$	500	0	NH_3^+	$NH_3 + h\nu \rightarrow NH_3^+ + e$, $J_{22} = 1.4 \times 10^{-8}$	$NH_3^+ + e \rightarrow NH_2 + H$, $K_{26} \sim 10^{-7}$,§ diffusion to ground
2.....	$N_2 = 10^{11}$, $Na = 5.3 \times 10^5$	340	0	Na^+	$Na + h\nu \rightarrow Na^+ + e$, $J_{23} = 1.5 \times 10^{-7}$	$Na^+ + e \rightarrow Na + h\nu$, $K = 3.2 \times 10^{-12} \times (250/T)^{1/2}$,‖ diffusion to ground
3.....	$NH_3 = 1.0 \times 10^{11}$ day, 3.0×10^8 night; $N_2 = 1.0 \times 10^9$; $Na = 3.3 \times 10^6$	500	0	Na^+	$Na + h\nu \rightarrow Na^+ + e$, $J_{23} = 1.5 \times 10^{-7}$	$Na^+ + e \rightarrow Na + h\nu$, $K = 3.2 \times 10^{-12} \times (250/T)^{1/2}$, diffusion to ground
4.....	$NH_3 = 5.0 \times 10^{10}$ day, 1.0×10^{10} night; $Na = 3.7 \times 10^6$	550	1×10^2 day, 5×10^2 night	Na^+	$Na + h\nu \rightarrow Na^+ + e$, $J_{23} = 1.5 \times 10^{-7}$	$Na^+ + e \rightarrow Na + h\nu$, $K = 3.2 \times 10^{-12} \times (250/T)^{1/2}$, diffusion to ground
5.....	$NH_3 = 3 \times 10^{10}$; $H = 5 \times 10^5, 1 \times 10^{10}$	500	0	Na^+	$Na + h\nu \rightarrow Na^+ + e$, $J_{23} = 1.5 \times 10^{-7}$, $H + h\nu \rightarrow H^+ + e$, $J = 8.4 \times 10^{-10}$	$Na^+ + e \rightarrow Na + h\nu$, $K = 3.2 \times 10^{-12} \times (250/T)^{1/2}$, $H^+ + NH_3 \rightarrow H + NH_3^+$, $K_{30} \sim 10^{-10}$#
6.....	$NH_3 = 3 \times 10^{11}$	~500	0	NH_3^+	$NH_3 + e \rightarrow NH_3^+ + e + e$, $NH_3 + p \rightarrow NH_3^+ + p + e$, $F_e(\infty) = 3 \times 10^7$	$NH_3^+ + e \rightarrow NH_2 + H$, $K_{26} \sim 10^{-7}$

* Models 1 and 5 are time independent.

† Number densities at the surface are given. Number densities at higher altitudes can be calculated from diffusive equilibrium.

‡ Mean J-values, calculated for zero optical depth.

§ Estimated.

‖ Bates and Dalgarno (1962).

Estimated from Coplan and Ogilvie 1969.

Model 2, shown in figure 12, gives good agreement with the observed daytime ionosphere. Ionization is removed in this case primarily by diffusion to the planetary surface, with some contribution due to radiative recombination. The ionosphere is composed primarily of Na^+, and the time constant for ionization loss is long, $\sim 10^6$ s, such that the ionosphere exhibits no significant diurnal variation. The model fails therefore to account for the nightside data and must be rejected on this basis.

Model 3 is more plausible, although here also there are deficiencies. Model 3 allows for more rapid diffusion of ionized species onto the planetary surface than does model 2. It assumes a large diurnal variation for the surface density of NH_3, taken to be the major component of the daytime atmosphere. The surface density of NH_3 is allowed to vary from a daytime value of 10^{11} cm^{-3} to a nightside value of 3×10^8 cm^{-3}. We assume that the atmosphere contains significant quantities of N_2, and take the surface density for this component as 10^9 cm^{-3}. We ignore

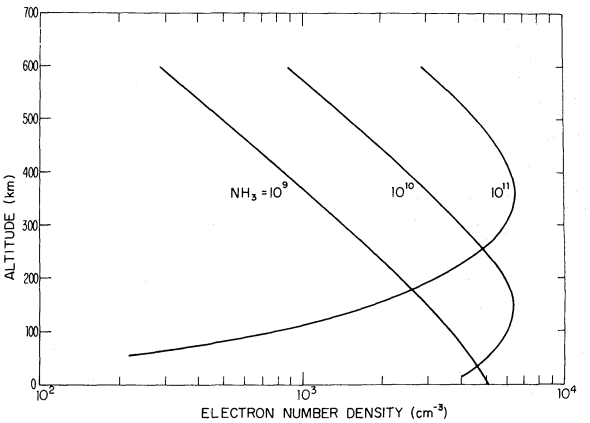

FIG. 11.—Electron number density profiles computed with model 1, assuming surface densities of NH_3 equal to 10^9, 10^{10}, and 10^{11} cm^{-3}. The atmosphere is assumed to be isothermal at 500° K.

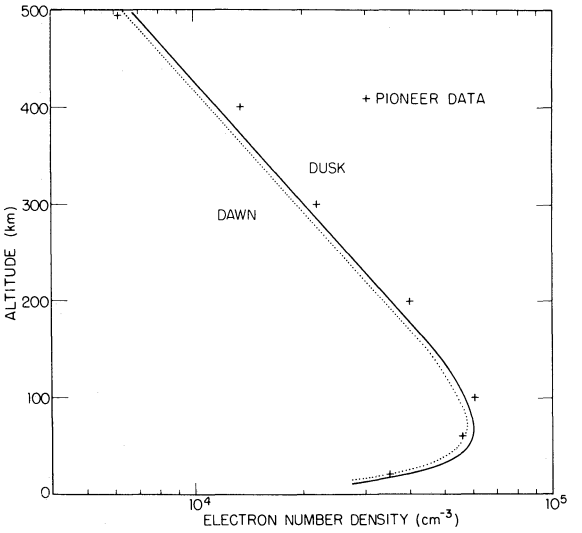

FIG. 12.—Electron number density profiles computed with model 2, with parameters given in table 1

possible time variations in the concentration of N_2 and note that the large diurnal variation of NH_3 invoked by model 3 could be a natural consequence of condensation processes which should be important for this gas at the cold surface temperatures which would apply on the nightside of the planet. The model properly accounts for the observed diurnal change in electron density at the ionospheric maximum. It also gives satisfactory results for the magnitude of the electron densities measured at the ionospheric peaks on both day and night sides of the planet. It fails, however, to reproduce the observed heights for the ionospheric maxima and also appears to give a trend for the peak height which is opposite in sense from the observed behavior. The height of maximum ionization in the model varies from a daytime value of about 40 km to a nighttime value of 150 km, in contrast to the observed behavior in which the height of the peak is lowered during the night from its daytime value of about 100 km to a late night value close to zero. As was the case for model 2, Na^+ is the dominant positive ion for all profiles shown in figure 13.

Ambipolar diffusion is the dominant loss process for ionization at all altitudes in models 2 and 3. The electron density at the ionospheric maximum is given by

$$-nw_d = \frac{nD}{H} = J[\mathrm{Na}]H' , \tag{18}$$

where J is the photoionization rate for sodium, [Na] is the sodium concentration at the maximum, and H' is the scale height for neutral sodium. The diffusion coefficient D is inversely proportional to the total density of neutral

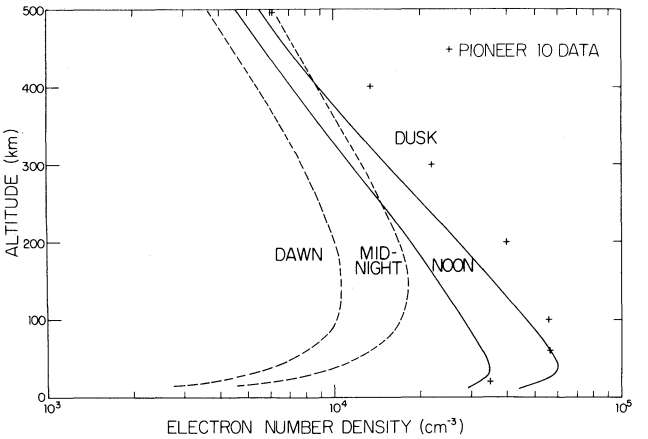

FIG. 13.—Electron number density profiles computed with model 3 with parameters given in table 1

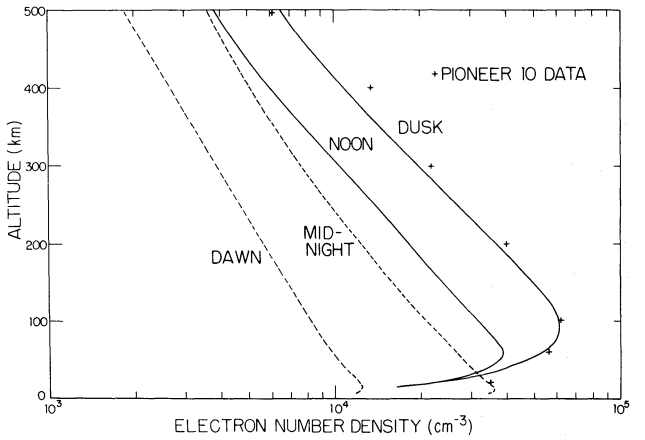

FIG. 14.—Electron density profiles computed with model 4 with parameters given in table 1

gas, N, and equation (18) can be used therefore to provide an estimate for the product $N_0[\mathrm{Na}]$. Extrapolating this result to the planetary surface, and using appropriate numerical values for D, H, J, and H', we find

$$N_0[\mathrm{Na}]_0 \simeq 10^{16}\ \mathrm{cm}^{-6}\,, \tag{19}$$

where N_0 and $[\mathrm{Na}]_0$ are the surface densities (cm^{-3}), of total gas and sodium, respectively. We can now use the upper limit derived earlier for the total column density of sodium, $10^{13}\ \mathrm{cm}^{-2}$, to set a lower bound for N_0. This analysis leads to the result $N_0 \geq 10^{10}\ \mathrm{cm}^{-3}$.

Results from model 4 are shown in figure 14. Model 4 allows for the possible presence of a finite vertical drift w_0. We take w_0 to be directed upward during the day, downward at night. The daytime velocity is set equal to $1\ \mathrm{m\ s}^{-1}$, and the nighttime velocity is chosen in such a manner as to conserve total mass for the bulk atmosphere. Vertical motions of the magnitude discussed here could arise due to evaporation and condensation of gases at the planetary surface—for example, NH_3, which we assume to be the dominant constituent of the neutral atmosphere. Alternatively, vertical motions could be generated by the electric field induced by the motion of Io through Jupiter's magnetic field. The model shown here is not unique. It is clear that acceptable solutions could be obtained with a variety of combinations for the choices of N_0, $[\mathrm{Na}]_0$, and w_0. Vertical motion in the bulk atmosphere provides an additional degree of flexibility which allows us to construct models for the ionosphere in accord with all of the major features exhibited by the *Pioneer 10* results. Thus model 4 properly accounts for the observed locations of the day and nightside ionospheric maxima, and also gives acceptable values for the electron densities at the maxima. The scale height for the nightside ionosphere can be adjusted readily by an appropriate change in the value assumed for the nightside atmospheric temperature. In the computations shown here we assumed that day and nightside temperatures were similar and adopted an isothermal model, at 500° K, for both day and nighttime atmospheres.

The temperature of the neutral atmosphere can be obtained by solving the appropriate energy equation

$$\frac{d}{dz}\left(K\frac{dT}{dz}\right) = h\,, \tag{20}$$

where K is the thermal conductivity coefficient, and h is the net volume heating rate.[2] The atmosphere is heated by absorption of sunlight in the primary reactions

$$h\nu + \mathrm{N_2} \rightarrow e + \mathrm{N_2^+}\,, \tag{21}$$

$$h\nu + \mathrm{NH_3} \rightarrow \mathrm{NH_3^+} + e\,, \tag{22}$$

$$h\nu + \mathrm{Na} \rightarrow \mathrm{Na^+} + e\,, \tag{23}$$

and

$$h\nu + \mathrm{NH_3} \rightarrow \mathrm{NH_2} + \mathrm{H}\,. \tag{24}$$

[2] We have omitted here possible contributions to the net heating or cooling rates at any given level due to expansion or contraction of the atmosphere. These contributions should be included in a more complete, time-dependent model for thermal structure.

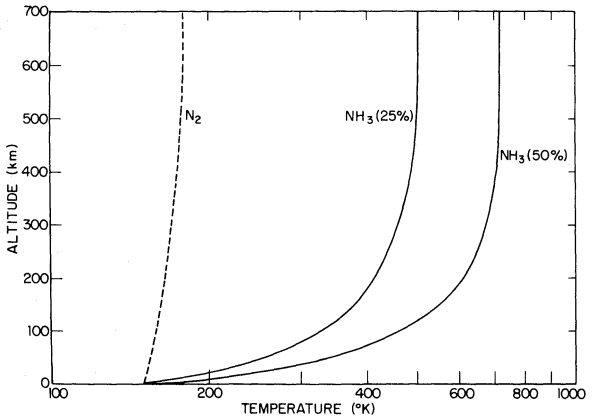

FIG. 15.—Temperature profiles computed with equation (20). The total density of neutral gas at Io's surface is taken as 10^{11} cm^{-3} for all models shown here.

The electrons in reactions (21)–(23) are formed with kinetic energy, as are the neutrals in reaction (24). Kinetic energy is released also by the recombination reactions

$$N_2^+ + e \rightarrow N + N\,, \tag{25}$$

$$NH_3^+ + e \rightarrow NH_2 + H\,, \tag{26}$$

and

$$NH_2 + H \rightarrow NH_3\,. \tag{27}$$

A quantitative estimate for the net atmospheric heating rate is difficult, and is scarcely justified here, given the major gaps in our knowledge of atmospheric composition. We shall assume that a certain fraction of the solar energy absorbed at any given altitude is converted locally to heat. This fraction is treated as an adjustable parameter to be varied in order to find the possible range of atmospheric temperatures.

Equation (20) was solved numerically subject to the boundary conditions

$$T(0) = 150^\circ\,\mathrm{K} \tag{28}$$

and

$$\frac{dT}{dz}(\infty) = 0\,. \tag{29}$$

These relations correspond to the requirements that the atmospheric temperature at $z = 0$ should be determined by collisions of gas molecules with the surface and that the conductive flux of heat should vanish at sufficiently high altitudes. A summary of results is shown in figure 15.

If the atmosphere is composed of N_2, we estimate an exospheric temperature of no more than 180° K, even if 100 percent of the absorbed sunlight is converted locally to heat. Including acceptable quantities of sodium would not lead to any significant change in this result. The flux of solar radiation at wavelengths absorbed by nitrogen, $\lambda < 800$ Å, is too low to provide major heating of the atmosphere. Ammonia absorbs sunlight at wavelengths less than 2400 Å, by reaction (24), and the available flux is much higher. We assume that the recombination reaction (27) does not proceed to any significant extent in the atmosphere and that atmospheric heating proceeds primarily by reaction (24). The energy available for atmospheric heating, per photon absorbed, is equal to the difference between the energy of the photon and the dissociation energy of NH_3. Some fraction of this energy may be used to produce excited radiating states of NH_2. The remainder is released as heat, and the curves in figure 15 assume efficiencies of 25 percent and 50 percent for conversion to kinetic energy in reaction (24). The resulting values for the exospheric temperature are 500° and 700° K, respectively, in good agreement with temperatures derived from analysis of the ionospheric data. A significant concentration of NH_3 is apparently required in order to account for the observed magnitude of the ionospheric scale height.

Ammonia can also play a useful role as a sink for protons in Io's atmosphere. Protons, formed by photoionization of hydrogen, may be removed by

$$H^+ + NH_3 \rightarrow H + NH_3^+\,, \tag{30}$$

and some such loss process is evidently required in order to suppress a major proton component in the ionosphere. The concentration of H^+ will increase with increasing height in regions of the atmosphere where H^+ is a minor ion. The variation with height is determined in part by the source and loss reactions, photoionization and charge

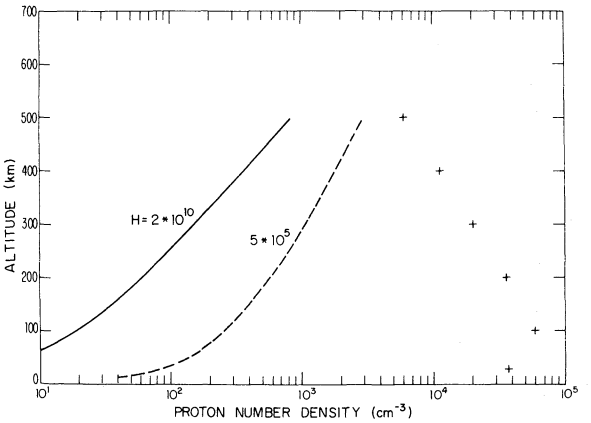

FIG. 16.—Proton number densities computed with model 5, assuming the parameters given in table 1. Solid line shows results with $k_{30} = 0$ and H number density at the surface $= 2 \times 10^{10}$ cm^{-3}. Dashed line shows results for $K_{30} = 10^{-10}$ cm^3 s^{-1}, with the surface density equal to 5×10^5 cm^{-3}. The *Pioneer 10* electron number density profile is indicated by the symbols +.

transfer, respectively, in part by diffusion, in which the dominant force on protons is that due to the polarization field established by the major ion. Distributions of H^+, with various assumptions for the surface density of atomic hydrogen, are shown in figure 16. The charge transfer reaction (30) was omitted in the computations represented by the dashed lines in the figure, and it is clear that in the absence of a rapid sink for H^+, the surface density of H must be exceedingly low, less than 10^6 cm^{-3}. As we shall see in the following section, it is difficult to account for the observed airglow at Lα with H concentrations of this magnitude. On the other hand, the surface concentration of H could be quite large, of order 10^{10} cm^{-3}, if NH_3 were a major constituent of the atmosphere and if the rate constant for (30) were also large, of order 10^{-10} cm^3 s^{-1}. The computations summarized by the solid curves in figure 16 assume a surface concentration of NH_3 equal to 3×10^{10} cm^{-3} and a rate constant for reaction (30) given by 10^{-10} cm^3 s^{-1}. The various curves in figure 16 are labeled by the values assumed for the surface concentration of H.

A quantitative assessment of the possible role of corpuscular radiation is difficult, given the present gaps in our understanding of Io and its environment. We can, however, define the conditions under which corpuscular radiation could make a major contribution to the observed ionization balance. Maximum ionization should occur at a height of approximately 100 km above the surface on the dayside. The flux of energetic particles entering the atmosphere on the nightside of the planet must be much smaller than the corresponding flux on the dayside, by at least a factor of 100. Heating rates associated with particle bombardment must be consistent with the observed ionospheric scale height; i.e., the net heating rate should be comparable to that which applied for the 500° K model in figure 15. These considerations suggest a net deposition of corpuscular energy of order 10^{11} eV cm^{-2} s^{-1}, or less, and the dayside ionization rate could be as large as 10^9 cm^{-2} s^{-1}.

The corpuscular ionization rate at any given level z would be given approximately by

$$q(z) = \frac{n(z)}{35} \int \mathscr{F}(E, z) E Q(E) dE , \tag{31}$$

where $n(z)$ is the number density (cm^{-3}) of neutral species at z, $\mathscr{F}(E, z)$ is the flux (cm^{-2} s^{-1} eV^{-1}) of energetic primaries between E and $E + dE$, E is the energy of primaries (eV), and $Q(E)$ is an appropriate cross section to describe the interaction of primaries with the bulk atmospheric gas. The factor 1/35 reflects an assumption that on average 35 eV are required to produce an ion-electron pair. The flux at z is given approximately by

$$\mathscr{F}(E, z) = \mathscr{F}(E, \infty) \exp [- Q(E) n(z) H] , \tag{32}$$

where H is the atmospheric scale height.

The analysis is simplified considerably if we restrict attention to monoenergetic primaries and adopt an effective value, α (cm^3 s^{-1}), for the electron-ion recombination coefficient. The electron density at z is given by

$$n_e(z) = \left[\frac{n(z)\mathscr{F}(\infty) E Q}{35\alpha}\right]^{1/2} \exp \left[-\frac{Q n(z) H}{2}\right] , \tag{33}$$

where $\mathscr{F}$ is the total flux (cm^{-2} s^{-1}). The electron density at the ionospheric maximum assumes the simple form

$$n_e^{\max} = 0.6 \left[\frac{F(\infty) E}{25 \alpha H}\right]^{1/2} , \tag{34}$$

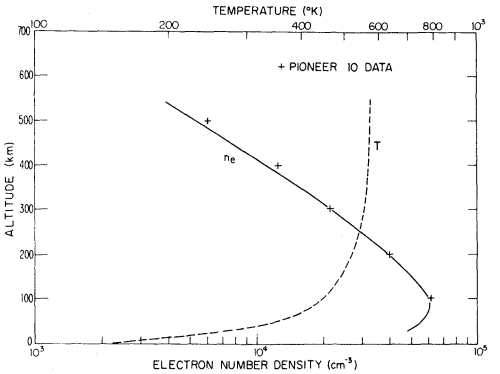

FIG. 17.—Electron number density and atmospheric temperature profiles computed with model 6 using equation (33), (20), and (35) and parameters given in table 1.

and the heating rate at z is given by

$$\mathrm{H}(z) = n(z)Q\frac{E}{4}F(\infty)\exp\left[-Qn(z)H\right]. \tag{35}$$

The factor $\frac{1}{4}$ reflects an assumption regarding the heating efficiency for energetic primaries.

Figure 17 shows electron density and atmospheric temperature computed using equations (33), (20), and (35). We adopted a cross section $Q = 10^{-18}$ cm^2, and the results shown here should be appropriate for incident electrons at 10 keV, or incident protons at 10 MeV. The surface number density, $n(0)$, for the bulk atmospheric gas was set equal to 3×10^{11}. The atmospheric scale height H was taken as 75 km, and the incident particle flux $F(\infty)$ had a value of 3×10^7.

The results can be scaled readily for different values of the incident energy, or for different values of $n(0)$. The cross section $Q(E)$ varies approximately as $(\log E)/E$. Thus an increase (or decrease) in $n(0)$ requires a corresponding increase (or decrease) in the energy of the primaries in order to maintain a fixed height for the maximum electron density. The flux of primaries at energy E required to account for the observed magnitude of the electron density at 100 km is given by

$$F(E) = 10^7\left[\frac{E_0\log(E/V_0)}{E\log(E_0/V_0)}\right], \tag{36}$$

with E_0 equal to 10 keV for electrons, 10 MeV for protons. If the observed ionosphere is formed primarily by corpuscular bombardment at energy E, the appropriate value for the surface density $n(0)$ should satisfy the relation

$$n(0) = 3 \times 10^{11}\left[\frac{E\log(E_0/V_0)}{E_0\log(E/V_0)}\right], \tag{37}$$

where, as before, E_0 is equal to 10 keV for electrons, 10 MeV for protons, and $V_0 \approx \frac{1}{4} \times$ ionization potential = 2.5 eV.

As may be inferred from figure 17, corpuscular radiation could provide a ready explanation for all features of the observed ionosphere. Model 6 is considered, therefore, as an alternative to model 4, and further work will be required to discriminate between these alternative explanations for the *Pioneer 10* data. In the interim, the fluxes $F(E)$ inferred here for various incident energies of monoenergetic protons and electrons can be regarded as upper limits to the possible corpuscular sources. Results for various assumed values of $n(0)$ are summarized in figure 18.

IV. EXCITATION OF LYMAN-α EMISSION

We discuss here some implications of the Lα observations reported by Judge and Carlson (1974). They found bright emission from the vicinity of Io such that the intensity could be as large as 10 kR if all of the emission were to originate in the satellite's atmosphere. It appears now (Judge 1974) that the observed radiation comes from an extended region of space around Io. The intensity is approximately 300 R, and the emission is observed to precede and follow Io as the satellite moves around its orbit. The radiating cloud has an angular size, measured with respect to Jupiter, of approximately 120°. The cloud was observed also as it passed through the shadow of Jupiter, and from these data it is clear that the cloud has a vertical extent, with respect to Io's orbital plane, of less than one Jovian diameter. The emission is most probably due to resonance scattering of sunlight. The observed behavior of the emission in the shadow region appears to preclude a major contribution due to particle impact.

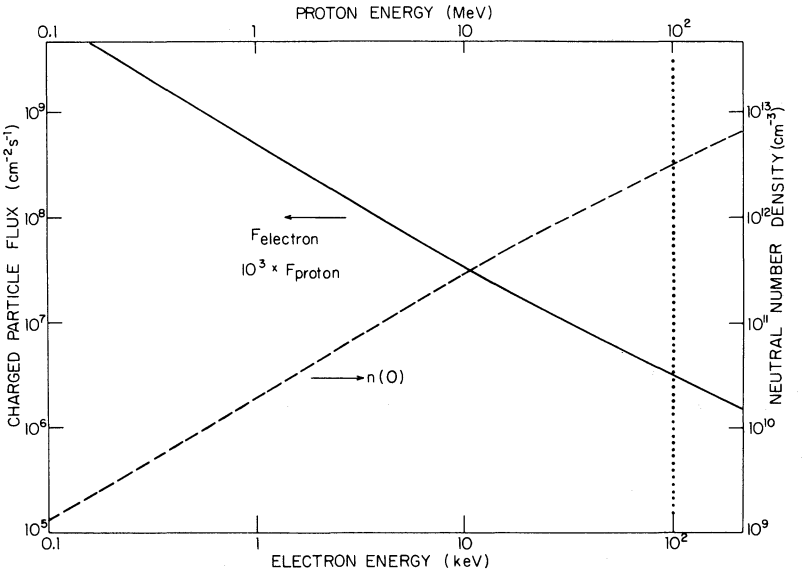

FIG. 18.—Flux of monoenergetic primary electrons or protons at energy E and the neutral number densities required to produce the observed characteristics of the ionosphere. Energy range to the right of the dotted line would require a neutral atmosphere exceeding the upper limit derived by Smith and Smith (1973).

Figure 19 shows Lα intensities predicted on the basis of resonance scattering, for two values of atmospheric temperature, 500° and 5000° K, and for two values of the surface reflectivity, 0 and 0.5. Results are shown as functions of τ_0, optical depth at the core of the Lα line. The upper horizontal scale gives the corresponding values for the column density of H. An intensity of 300 R implies a column concentration of H, along the line of sight, of order 10^{13} atoms cm^{-2} s^{-1}. This result is essentially independent of assumptions regarding the surface reflectivity or the temperature of the medium. The curves with $r = 0$ should be most appropriate for scattering in the diffuse cloud, and the ionospheric analysis described in the preceding section suggests that 500° K should be a reasonable estimate for the cloud temperature.

The hydrogen atoms measured in the diffuse cloud presumably originate at Io and are most probably emitted from the satellite's atmosphere by thermal Jeans escape. The velocity required for an atom to escape Io's gravitational field is only 2.5 km s^{-1}, which may be compared with the mean thermal velocity of 2.9 km s^{-1} that would

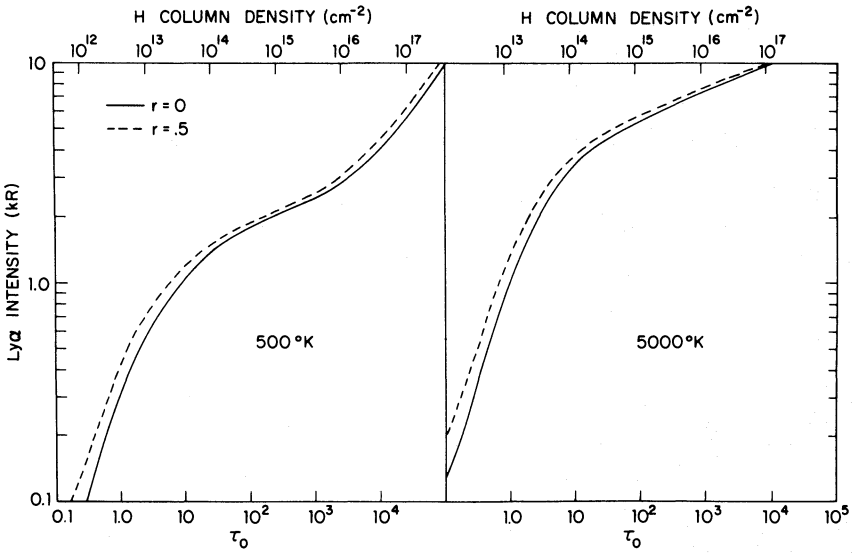

FIG. 19.—Intensity of Lα emission due to resonance scattering of sunlight as a function of the H abundance expressed both in terms of optical depth at the line center and total column density. Results are presented for surface reflectivities $r = 0$ (*solid line*) and $r = 0.5$ (*dashed line*) and for temperatures 500° and 5000° K.

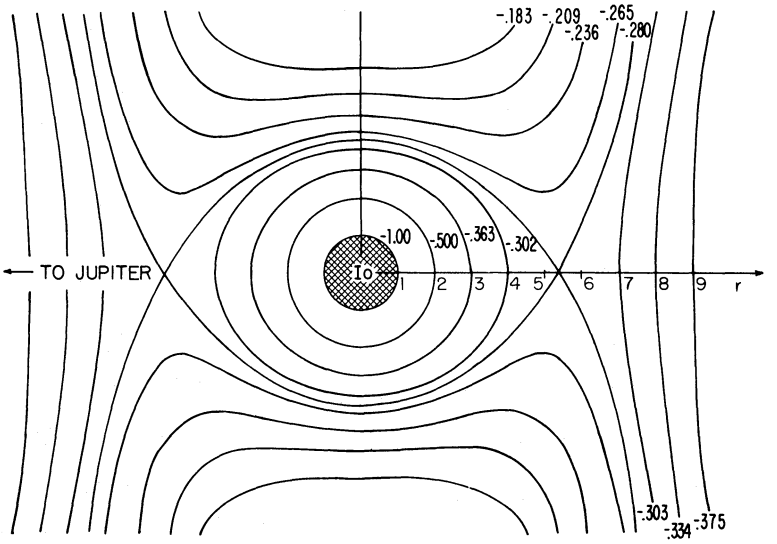

FIG. 20.—Gravitational equipotential surfaces in the vicinity of Io. The numbers give the magnitude of the potential measured in units of GM_{Io}/r_{Io} defined by $\phi(r, \theta) = -(1/r + \epsilon r^2 \cos^2 \theta)$, with

$$\epsilon = \frac{3}{2}\frac{M_J}{M_{Io}}\left(\frac{r_{Io}}{d}\right)^3,$$

where M_J = mass of Jupiter, M_{Io} = mass of Io, d = distance between Jupiter and Io, and r_{Io} = radius of Io. The quantity r defines the radial distance from Io in units of r_{Io}; θ is the polar angle taken as 0 in the direction of Jupiter. The solid body of Io is indicated by the shaded disk.

apply for a gas of hydrogen atoms at 500° K. Atoms are therefore emitted from Io with a significant velocity with respect to the parent body. Their subsequent history depends on the details of the gravitational potential surfaces near Io. These surfaces are illustrated schematically in figure 20,[3] and limits placed by Judge and Carlson (1974) on the vertical extent of the hydrogen cloud can be readily adopted to derive a corresponding limit for the lifetime of hydrogen near Io's orbit. In this manner we estimate a lifetime for atomic hydrogen of order 10^5 s, a result which may be compared with the calculated value of approximately 10 years for the photoionization lifetime of the gas. It seems clear that an additional loss process must be invoked for hydrogen, and the symmetrically resonant reaction

$$H^+ \text{ (hot)} + H \rightarrow H \text{ (hot)} + H^+ \tag{38}$$

is the most obvious candidate. The hydrogen lifetime, as determined by charge transfer with protons of energy E, would be given by

$$\tau = \{F(E)Q(E)\}^{-1} \tag{39}$$

where $F(E)$ is the flux ($cm^{-2}\,s^{-1}$) of hot protons and $Q(E)$ is the corresponding cross section. Values of $F(E)$ required to account for the empirical lifetime of 10^5 s are summarized in table 2. Evidently the Lα observations

TABLE 2

FLUX OF PROTON AT ENERGY E REQUIRED TO ACCOUNT FOR THE LIFETIME OF HYDROGEN CLOUD

E(eV)	$Q(E)$(cm^{-2})	$F(E)$($cm^{-2}\,s^{-1}$)
1.....	4.9×10^{-15}	2.0×10^{9}
10.....	4.0×10^{-15}	2.5×10^{9}
10^2.....	2.7×10^{-15}	3.7×10^{9}
10^3.....	1.8×10^{-15}	5.5×10^{9}
10^4.....	0.9×10^{-15}	1.1×10^{10}
10^5.....	1.0×10^{-17}	1.0×10^{12}

[3] McElroy *et al.* (1974) gave a plot of the static gravitational field near Io. The escape process is more accurately represented by the total gravitational potential surfaces shown in figure 20.

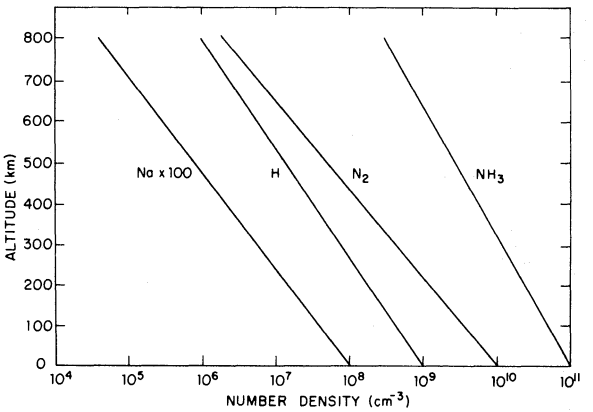

FIG. 21.—Model for Io's neutral atmosphere, as discussed in the text

could be understood if the flux of 10-eV protons at Io's orbit had the value 2.5×10^9 cm^{-2} s^{-1}, i.e., if the density of 10-eV protons were of order 10^3 cm^{-3}. As indicated by the table, somewhat larger fluxes would be required if the lifetime of hydrogen were set primarily by collisions with more energetic protons. In particular we note that the fluxes measured by Simpson *et al.* (1974), by Trainor *et al.* (1974), and by Fillius and McIlwain (1974), for protons with energies greater than 500 keV, are too low to play a significant role in the removal of neutral hydrogen.

The observed dimensions of the hydrogen cloud, and the measured intensity of Lα, can be used to obtain an estimate for the total abundance of hydrogen around Io. This analysis, in combination with the lifetime derived above, allows us to compute the magnitude of the hydrogen escape flux from Io. The hydrogen abundance is uncertain to some extent due to the lack of precise information on the vertical dimensions of the cloud. The escape flux, however, should be reasonably well defined, since the analysis in this case is essentially independent of the value assumed for the vertical dimension, L.[4] Adopting a value for L equal to one Jovian radius, approximately 7×10^4 km, we estimate that the cloud should contain a total concentration of 1.5×10^{33} hydrogen atoms. The flux at Io required to maintain the extended cloud must be of the order of 10^{11} atoms cm^{-2} s^{-1} and could be supplied by photolysis of NH_3. It is difficult to escape the conclusion that Io's atmosphere must contain significant concentrations of a hydrogenic gas which can be readily decomposed by incident sunlight. Ammonia is the most obvious candidate, and the required column density should be of order 10^{18} molecules cm^{-2}, consistent with the earlier discussion of possible models for the ionosphere.

If we assume that Io's exospheric temperature has the value 500° K implied by the ionospheric data, we can use the escape flux derived above to compute the density of hydrogen at the critical level. The density at higher levels can be computed readily by using the exospheric theory presented by Chamberlain (1963), and the density at lower altitudes can be derived by solving the appropriate diffusion equation given by

$$\phi(z) = -D\left(\frac{\partial n}{\partial z} + \frac{n}{H}\right), \tag{40}$$

where all symbols have their customary significance. The flux ϕ at height z is approximately equal to the total column production rate (cm^{-2} s^{-1}) for hydrogen due to photolysis of NH_3 at levels below z and is given by

$$\phi(z) = \int_0^z J(z)[NH_3]dz\,. \tag{41}$$

Results for H are shown in figure 21, which gives a detailed model for Io's atmosphere consistent with all of the constraints discussed in this paper. The intensity of Lα airglow, excited by resonance scattering of sunlight, would be of order 1 kR if figure 21 were indeed an appropriate representation of conditions in Io's atmosphere.

Airglow at Lα can be excited also by a variety of reactions involving energetic particles. Energetic protons can contribute by reactions such as

$$H^+ + NH_3 \rightarrow H(2p) + NH_3^+ \tag{42}$$

$$\rightarrow H^+ + H(2p) + NH_2 \tag{43}$$

$$\rightarrow H + H(2p) + NH_2^+\,, \tag{44}$$

[4] The rate, in atoms s^{-1}, required to supply the observed cloud, is proportional to the total number of atoms, $\mathcal{N}$, in the cloud, and inversely proportional to the lifetime, τ, for atoms in the cloud. Both $\mathcal{N}$ and τ, at least in the framework of the present discussion, vary linearly with L, the vertical dimension of the cloud.

followed by

$$H + NH_3 \rightarrow H + H(2p) + NH_2 \quad (45)$$

$$\rightarrow H + H(2p) + NH_2^+ + e \quad (46)$$

$$\rightarrow H^+ + H(2p) + NH_2 + e \quad (47)$$

$$\rightarrow H(2p) + NH_3 ; \quad (48)$$

or by

$$H^+ + N_2 \rightarrow H(2p) + N_2^+ , \quad (49)$$

followed by

$$H + N_2 \rightarrow H(2p) + N_2^+ + e \quad (50)$$

$$\rightarrow H(2p) + N + N^+ + e \quad (51)$$

$$\rightarrow H(2p) + N_2 . \quad (52)$$

Energetic electrons are similarly effective by reactions such as

$$e + NH_3 \rightarrow e + NH_2 + H(2p) \quad (53)$$

$$\rightarrow 2e + NH_2^+ + H(2p) . \quad (54)$$

The intensity of Lα airglow associated with particle bombardment of the atmosphere could be as large as 10 kR, if we adopt the upper limits to the particle fluxes derived in the preceding section. The intensity of Lβ excited by resonance scattering of sunlight would be of order 100 R, and the corresponding value for the intensity associated with the corpuscular mechanism could be as large as 2 kR. The intensity of Hα airglow excited by fluorescent scattering of solar Lβ would be of order 20 R, and the intensity due to corpuscular bombardment could be as large as 200 R.

Photolysis of NH_3 provides an important source of nitrogen-bearing radicals in Io's atmosphere. There are two obvious end products for NH_3 photolysis: production of $NaNH_2$ or production of N_2. If $NaNH_2$ is important, one might expect significant concentrations of condensed $NaNH_2$ on the satellite's surface. Any N_2 produced must eventually escape from the atmosphere, and the escape flux could be as large as 10^{11} cm^{-2} s^{-1}. Thermal escape of N_2 would be exceedingly inefficient at 500° K. The maximum possible escape flux at this temperature would be of order 10^4 molecules cm^{-2} s^{-1}, and it is similarly difficult to supply the extended sodium cloud if 500° K is a representative temperature for all times in Io's atmosphere. We may recall, however, that the sodium emission is a sporadic phenomenon, and that the temperature implied by Brown and Chaffee's (1974) data is apparently very high, in excess of 5000° K (McElroy *et al.* 1974). A temperature of 10,000° K, present for as little as 20 percent of the time, could account for an average escape flux of N_2 as large as 10^{11} molecules cm^{-2} s^{-1}. The corresponding escape flux for Na would have an average value of order 10^7 atoms cm^{-2} s^{-1} if the Na concentration were maintained at the levels indicated by figure 21. We assume that the energy source required to raise the atmospheric temperature to the values implied by the sodium emission measurements must be derived from the electromagnetic interaction of Io with the external Jovian environment. The atmosphere would cool rapidly once the heat source was removed. The primary mechanisms for energy loss are radiation of the sodium D lines, conduction of heat to the satellite's surface, and evaporation of gases to space.

Io could play an important role for Jupiter's magnetosphere, acting both as a source and as a sink for the trapped charged particles. The charge transfer reaction (38) transforms a fast proton into a fast hydrogen atom. If the fast proton has an initial energy greater than 10 eV, the product hydrogen atom could escape from the Jovian system. The proton sink due to this process could be as large as 10^{28} ions s^{-1}, and the corresponding energy sink could exceed 10^{29} eV s^{-1}. Atoms produced by charge transfer with protons of energy less than 10 eV would be free to move to large distances from Jupiter, where they would be eventually ionized by sunlight, providing an extensive source of trapped particles. These particles could be responsible in part for the observed distortion of Jupiter's dipole magnetic field at distances in excess of 5 Jovian radii (Van Allen *et al.* 1974). Photoionization of hydrogen could also provide an important source of magnetospheric energy, since the electrons formed in this manner are released with initial mean energy of approximately 10 eV. Charge transfer between fast protons and cold hydrogen atoms could provide an important sink for energetic protons near Io's orbit. If we assume that the observed hydrogen cloud has a horizontal thickness of approximately 2 Jovian radii, we estimate that the hydrogen density should be of order 10^2 cm^{-3}. The lifetime of protons in this cloud would be given by

$$\tau = (vnQ)^{-1} ,$$

where v is the proton velocity, n is the hydrogen density, and Q is an appropriate cross section. Lifetimes versus

TABLE 3
LIFETIME OF JOVIAN PROTONS IN Io'S HYDROGEN CLOUD

E(eV)	Q_{cc}(cm^2)	Q_I(cm^2)	τ_{cc}(s)	τ_I(s)	τ(s)
10^3	2×10^{-15}	...	2×10^5	...	2×10^5
10^4	10^{-16}	...	1×10^5	...	1×10^5
10^5	10^{-17}	10^{-16}	3×10^6	3×10^5	3×10^5
10^6	10^{-21}	10^{-17}	10^{10}	1×10^6	1×10^6
10^7	...	10^{-18}	...	3×10^6	3×10^6

NOTE.—Q_{cc}: $H^+ + H \rightarrow H + H^+$ (Rapp and Francis 1962); Q_I: $H^+ + H \rightarrow 2H^+ + e$ (Fite *et al.* 1960).

charge transfer are given as a function of energy in table 3. The table also includes lifetimes computed using the total cross section for proton-hydrogen scattering.

V. CONCLUDING REMARKS

Our understanding of Io—its atmosphere, surface, and environment—remains at a rudimentary state, although considerable advances have taken place in the past year. The sodium emission provides a powerful tool for remote sensing of Io, and there seems little doubt that further observations of this phenomenon can provide new insights into the complex physical and chemical processes that regulate conditions in the Jovian system. There are several unresolved questions, which we shall address briefly in the discussion that follows. These questions relate to the origin of atmospheric sodium, the nature of the excitation process, and the mechanism for atmospheric escape.

Matson *et al.* (1974) drew attention to the possible role of sputtering as a release mechanism for bound surface sodium. Sputtering would be induced by energetic particle bombardment of Io's surface. These particles could originate either in Jupiter's magnetosphere, or in Io's atmosphere, where they might be accelerated by local electric fields. The latter possibility is speculative and, although potentially important, cannot be quantitatively assessed until detailed models are developed for the interaction of Io with its external environment. The analyses in §§ III and IV place strong constraints on the nature and density of Io's atmosphere, and it is difficult to avoid the conclusion that the total column density of atmospheric gas must be at least as large as 10^{18} molecules cm^{-2}. In this case Io's surface would be to some extent shielded from the trapped Jovian radiation, and only particles at the highest energies could penetrate directly from the magnetosphere to the satellite's surface. We estimate that the cutoff energies for protons and electrons should be of order 10 MeV and 10 keV, respectively. Despite these restrictions, sputtering induced by magnetospheric particles could be important. The yield could be as large as 10^7 atoms cm^{-2} s^{-1}, and indeed sputtering is the only plausible mechanism identified so far to account for the presence of atmospheric sodium.

We derived earlier an estimate of 2×10^7 atoms cm^{-2} s^{-1} for the sodium source strength required to supply the observed sodium cloud. This estimate was based on two key assumptions. We assumed that resonance scattering of sunlight was the operative mechanism for excitation of the D lines in the extended cloud, and we assumed further that the lifetime of sodium was limited by photoionization. The sporadic nature of the emission would seem to suggest that either, or both, of these assumptions must be in error. Charge transfer with ambient protons could lead to some reduction in the sodium lifetime. A significant effect, however, would require a cross section in excess of 10^{-15} cm^2, an improbable result for low energy H^+–Na collisions. It seems more likely that the sporadic nature of the emission should be associated with a time variation in the excitation process. In this case resonance scattering of sunlight would play a relatively minor role, a conclusion reached earlier from consideration of the observed values for the ratio of line intensities D_2/D_1. With this model the extended cloud should be visible only at times when the planetary source was operative. The radiation observed to emanate from the extended cloud would be excited by collisional processes in the atmosphere, and the planetary radiation would be subsequently scattered by the external medium. The sodium source at Io's surface required to supply the cloud could then be much smaller than the value quoted above, and the requirements for the sputtering source should be reduced accordingly.

McElroy *et al.* (1974) offered the hypothesis that the sodium on Io's surface might be present in solution with solid ammonia. There are several problems with this idea, as discussed, for example, by Matson *et al.* (1974), who drew attention to the apparent absence of ice absorption features in the infrared spectrum of Io. Matson *et al.* argued also that hydrated ammonia should be more probable than pure ammonia ice, as indicated by the models developed by Lewis (1971). Neither objection is overwhelming. The presence of significant concentrations of dissolved sodium in the ammonia ice would make the solution electrically conducting and would wash out absorption features which might be exhibited by the pure ice form. If the surface ammonia were to originate at depth in Io's crust, it could be initially present in the hydrated form, but could be purified by cold trapping of the water before the ammonia emerged from the satellite's interior, a possibility communicated to us by J. Lewis. There are, however, other possibilities for the surface composition (Fanale *et al.* 1974). The analysis of the Lα airglow given here strongly suggests, in any event, that there must be a major concentration of a hydrogen-rich, condensable, molecular gas in Io's atmosphere. Ammonia is an obvious candidate, although NH_4SH is a further possibility.

If the sodium escape rate could be established, it should be possible to derive a reasonable estimate for the abundance of N_2 in Io's atmosphere. The sodium concentrations shown in figure 20 were determined on the basis of considerations outlined in § III. Sodium and nitrogen have comparable masses, and their effusion velocities should be similar for any plausible model describing atmospheric escape. If we adopt the escape flux for N_2 suggested by the analysis in § IV, we estimate a surface density for N_2 of order $4 \times 10^{17}\,\mathscr{F}^{-1}$, where $\mathscr{F}$ is the escape flux for sodium. If we take $\mathscr{F} \approx 3 \times 10^6\ \mathrm{cm^{-2}\ s^{-1}}$, equivalent to the assumption that resonance scattering of sunlight accounts for approximately 10 percent of the observed sodium emission, we calculate surface densities for N_2 of order $10^{11}\ \mathrm{cm^{-3}}$. The curve for N_2 included in figure 21 reflects this procedure.

It is important to place some observational limits on the fraction of the sodium radiation which is excited by scattering of sunlight. A measurement of the polarization of the emitted radiation would be particularly valuable, and an observational program designed to obtain these data has been initiated by F. Murcray, R. Goody, and R. Brown at this institution. It is important also to define accurately the intensity, time variability, and spatial extent of the sodium radiation. If possible, the observing program should incorporate high spectral resolution. The width of the individual D lines and its variation with space and time are key inputs to any critical analysis of the excitation conditions. It would be particularly valuable to search for a correlation of the optical phenomenon with Jupiter's decametric activity. We might note also that the emission should be correlated with orbital position if resonance scattering of sunlight were an important process. The scattering efficiency changes by as much as a factor of 10 due to the corresponding change in the Doppler shift with respect to incident sunlight.

The analysis in § IV depended critically on the observed dimensions of the hydrogen cloud detected by Judge and Carlson (1974). Further ultraviolet observations of Jupiter's Galilean satellites are clearly of high priority. The capabilities of the *Pioneer 11* instrument should be enhanced to allow a search for other gases in Io's environment; N_2, H_2, O, NH_3, H_2O, and perhaps Mg are obvious candidates. A ground-based telescopic search for Ca, H, and N_2 would also be valuable. The search could focus on emissions at 4226 Å (Ca), 6562 Å (H), 3914 and 4278 Å (N_2^+), and 5199 Å (N). Infrared observations with high spectral resolution, coupled with appropriate laboratory studies, would limit the range of speculation regarding the composition of Io's surface. In this context we might draw attention to the feature detected by Hansen (1972) and Morrison, Cruikshank, and Murphy (1972) near 10 μ which is apparently not due to atmospheric NH_3 (Hansen 1974) as suggested earlier by Sinton (1973).

We are indebted to R. W. Carlson, D. L. Judge, A. Kliore, S. I. Rasool, J. A. Simpson, and J. H. Wolfe for informative discussions of the *Pioneer 10* data. We acknowledge also the patience and stimulation of various colleagues, particularly R. A. Brown, H. Ehrenreich, R. M. Goody, and S. C. Wofsy, who bore with us during the course of this research. The work was supported by the Atmospheric Sciences Section of the National Science Foundation under grant GA-33990X to Harvard University. We also acknowledge partial support from the National Aeronautics and Space Administration contract NGL 22-007-228 to Harvard University.

APPENDIX

The emergent intensity of radiation emitted at zenith angle $\theta = \cos^{-1}\mu$ can be readily calculated using the exact relation

$$I_\lambda(0,\mu) = \int \frac{ds}{\mu}\, e^{-s/u} J(s)\,. \tag{A1}$$

The mean intensity $\bar{I}(s)$ and the source function $J(s)$ at optical depth s are given by

$$\begin{aligned}
\bar{I}_\lambda^{A}(S) &= \tfrac{1}{2}\epsilon(3^{1/2}C_1 S + D_1)\,, && 0 \le S \le \tau(\lambda)\,,\\
&= \tfrac{1}{2}\epsilon(-3S^2 + 3^{1/2}A_1 S + B_1)\,, && \tau(\lambda) \le S \le \tau(\lambda) + \Delta\tau(\lambda)\,;\\
J_\lambda^{A}(S) &= \bar{I}_\lambda^{A}(S)\,, && 0 \le S \le \tau(\lambda)\,,\\
&= \bar{I}_\lambda^{A}(S) + \epsilon\,, && \tau(\lambda) \le S \le \tau(\lambda) + \Delta\tau(\lambda)\,; \qquad \text{(A2)}\\
\bar{I}_\lambda^{B}(S) &= \tfrac{1}{2}\epsilon(-3S^2 + 3^{1/2}A_2 S + B_2)\,, && 0 \le S \le \Delta\tau(\lambda)\,,\\
&= \tfrac{1}{2}\epsilon(3^{1/2}C_2 S + D_2)\,, && \Delta\tau(\lambda) \le S \le \Delta\tau(\lambda) + \tau(\lambda)\,;\\
J_\lambda^{B}(S) &= \bar{I}_\lambda^{B}(S) + \epsilon\,, && 0 \le S \le \Delta\tau(\lambda)\,,\\
&= \bar{I}_\lambda^{B}(S)\,, && \Delta\tau(\lambda) \le S \le \Delta\tau(\lambda) + \tau(\lambda)\,; \qquad \text{(A3)}
\end{aligned}$$

$$\bar{I}_\lambda^{C}(S) = F\left[-\tfrac{3}{4}e^{-S} + \frac{\sqrt{3}}{2}A_3 S + \frac{A_3}{2} + \tfrac{1}{4}(\sqrt{3}+3)\right],\quad 0 \le S \le \tau(\lambda)\,;$$

$$J_\lambda^{C}(S) = \bar{I}_\lambda^{C}(S) + \tfrac{1}{4}Fe^{-S}\,, \tag{A4}$$

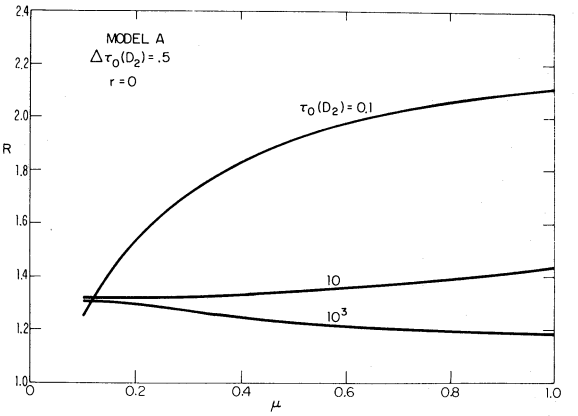

FIG. 22.—D_2 to D_1 intensity ratio R versus μ, the cosine of the zenith angle, computed with model A for $r = 0$, $\Delta\tau_0(D_2) = 0.5$, and $\tau_0(D_2) = 0.1, 10, 10^3$.

for models A, B, and C, respectively, if we use the two-stream approximation to solve the appropriate transfer equation.

The corresponding expressions for the emergent intensity are

$$I_\lambda^A(0,\mu) =$$

$$\epsilon\left(\frac{\sqrt{3}}{2}\mu C_1 + \frac{D_1}{2} - \left(\frac{\sqrt{3}}{2}[\tau(\lambda)+\mu]C_1 + \frac{D_1}{2} + \tfrac{3}{2}[\tau^2(\lambda) + 2\mu\tau(\lambda) + 2\mu^2] - \frac{\sqrt{3}}{2}A_1[\tau(\lambda)+\mu] - \left(\frac{B_1}{2}+1\right)\right)e^{-\tau(\lambda)/\mu}\right.$$

$$\left. + \left[\left[\tfrac{3}{2}\{[\tau(\lambda)+\Delta\tau(\lambda)]^2 + 2\mu[\tau(\lambda)+\Delta\tau(\lambda)] + 2\mu^2\} - \frac{\sqrt{3}}{2}A_1[\tau(\lambda)+\Delta\tau(\lambda)+\mu] - \left(\frac{B_1}{2}+1\right)\right]\right]e^{-[\tau(\lambda)+\Delta\tau(\lambda)]}\right), \quad \text{(A5)}$$

where

$$A_1 = C_1 + 2\times 3^{1/2}\tau(\lambda), \quad \text{(A6)}$$

$$B_1 = C_1 - 3\tau^2(\lambda), \quad \text{(A7)}$$

$$C_1 = 3^{1/2}\Delta\tau(\lambda)\frac{2(1+r) + (1-r)3^{1/2}\Delta\tau(\lambda)}{2 + (1-r)3^{1/2}[\Delta\tau(\lambda)+\tau(\lambda)]}, \quad \text{(A8)}$$

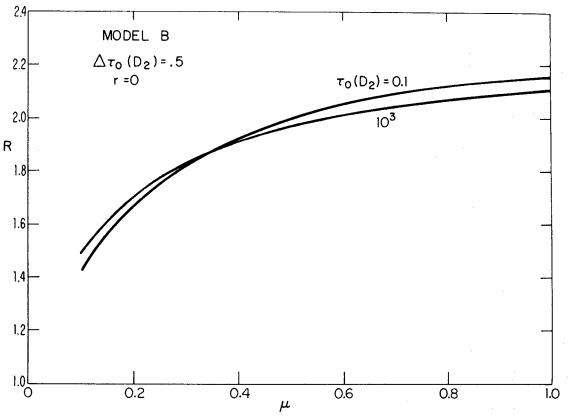

FIG. 23.—D_2 to D_1 intensity ratio R versus μ, the cosine of the zenith angle, computed with model B for $r = 0$, $\Delta\tau_0(D_2) = 0.5$, and $\tau_0(D_2) = 0.1, 10^3$.

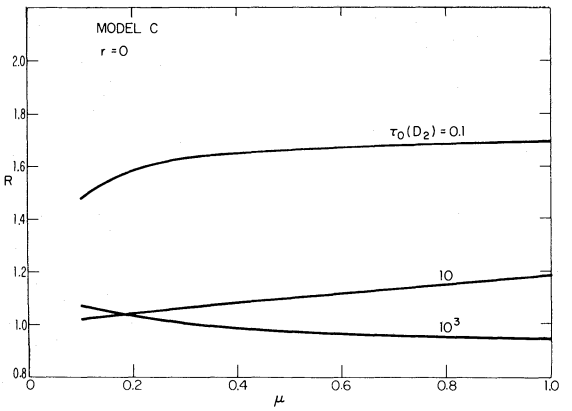

FIG. 24.—D_2 to D_1 intensity ratio R versus μ, the cosine of the zenith angle, computed for model C for $r = 0$ and $\tau_0(D_2) = 0.1$, 10, 10^3.

and

$$D_1 = C_1\,; \tag{A9}$$

$$I_\lambda^B(0,\mu) = \epsilon\Big[\Big[-3\mu^2 + \frac{\sqrt{3}}{2}A_2\mu + \Big(\frac{B_2}{2}+1\Big) + \Big(\frac{3}{2}[\Delta\tau^2(\lambda) + 2\mu\Delta\tau(\lambda) + 2\mu^2] - \frac{\sqrt{3}}{2}A_2[\Delta\tau(\lambda)+\mu] - \Big(\frac{B_2}{2}+1\Big) + \frac{\sqrt{3}}{2}C_2[\Delta\tau(\lambda)+\mu] + \frac{D_2}{2}\Big)e^{-\Delta\tau(\lambda)/\mu} - \Big(\frac{\sqrt{3}}{2}C_2[\Delta\tau(\lambda)+\tau(\lambda)+\mu] + \frac{D_2}{2}\Big)e^{-(\Delta\tau(\lambda)+\tau(\lambda))/\mu}\Big]\Big], \tag{A10}$$

where

$$A_2 = 3^{1/2}\Delta\tau(\lambda)\,\frac{2(1+r) + (1-r)3^{1/2}[\Delta\tau(\lambda) + 2\tau(\lambda)]}{2 + (1-r)3^{1/2}[\Delta\tau(\lambda)+\tau(\lambda)]}\,, \tag{A11}$$

$$B_2 = A_2\,, \tag{A12}$$

$$C_2 = 3^{1/2}\Delta\tau(\lambda)\,\frac{(1-r)[3^{1/2}\Delta\tau(\lambda) - A_2 - 2]}{(1+r) + (1-r)[1+3^{1/2}\tau(\lambda)]}\,, \tag{A13}$$

and

$$D_2 = -3^{1/2}\Delta\tau(\lambda)\,\frac{\{1 + r + (1-r)3^{1/2}[\Delta\tau(\lambda)+\tau(\lambda)]\}[3^{1/2}\Delta\tau(\lambda) - A_2 - 2]}{1 + r + (1-r)[1+3^{1/2}\tau(\lambda)]}\,; \tag{A14}$$

and

$$I_\lambda^C(0,\mu) = F_\lambda\Big\{\Big[\tfrac{1}{4}(\sqrt{3}+3) + \frac{A_3}{2}\Big](1 - e^{-\tau(\lambda)/\mu}) + \frac{\sqrt{3}}{2}A_3[\mu - (\mu + \tau(\lambda)\,e^{-\tau(\lambda)/\mu}] - \frac{1}{2}\frac{1}{1+\mu}\exp\Big[-\tau(\lambda)\Big(1+\frac{1}{\mu}\Big)\Big]\Big\}\,, \tag{A15}$$

with

$$A_3 = -\frac{\sqrt{3}}{2}\,\frac{(1+r)e^{-\tau(\lambda)} + (1-r)[1 + 3^{1/2}(1 - e^{-\tau(\lambda)})]}{2 + (1-r)3^{1/2}\tau(\lambda)}\,. \tag{A16}$$

Ratios of emergent line intensities, R, are shown as functions of μ for selected values of the parameters $\Delta\tau_0$, and τ_0, in figures 22–24. The discussion in the main body of this paper, which emphasized calculations with $\mu = 3^{-1/2}$, is not seriously restricted by the lack of detailed attention given to the possible variation of emergent intensity with μ. In particular, it is difficult to escape the conclusion reached earlier, that a strong internal source must be invoked in order to account for the large values, $\sim$2.0, observed for the intensity ratio R in the extended sodium cloud.

REFERENCES

Bates, D. R., and Dalgarno, A. 1962, *Atomic and Molecular Processes* (London: Academic Press), pp. 245–271.

Bates, D. R., and Patterson, T. N. L. 1962, *Planet. and Space Sci.*, **9**, 599.

Brown, R. A. 1973, in *Exploration of the Planetary System, Proceedings IAU Copernicus Symposium 4 (IAU Symposium 65)*, ed. A. Woszczyk and C. Iwaniszewska, in press.
Brown, R. A., and Chaffee, F. H., Jr. 1974, *Ap. J. (Letters)*, **187**, L125–L126.
Chamberlain, J. W. 1963, *Planet. and Space Sci.*, **11**, 901.
Coplan, M. A., and Ogilvie, K. W. 1969, *Sixth International Conference on Physics of Electronic and Atomic Collisions*, (Cambridge: MIT Press).
Fanale, E. P., Johnson, T. V., and Matson, D. L. 1974, to be published.
Fillius, R. W., and McIlwain, C. E. 1974, *Science*, **183**, 314.
Fite, W. L., Stebbings, R. F., Hummer, D. G., and Brackmann, R. T. 1960, *Phys. Rev.*, **119**, 663.
Hansen, O. L. 1972, *Bull. AAS*, **4**, 367.
———. 1974, *Ap. J. (Letters)*, **188**, L31.
Hunten, D. M. 1965, *J. Atm. Terr. Phys.*, **27**, 583–586.
Judge, D. L. 1974, private communication.
Judge, D. L., and Carlson, R. W. 1974, *Science*, **183**, 317–318.
Kliore, A. J., Cain, D. L., Levy, G. S., Eshleman, R., and Drake, F. D. 1965, *Science*, **149**, 1243.
Kliore, A., Cain, D. L., Fjeldbo, G., Seidel, B. L., and Rasool, S. I. 1974, *Science*, **183**, 323.
Kliore, A. J., Fjeldbo, G., Seidel, B. L., Sweetnam, D. N., Sesplaukis, T. T., Woiceshyn, P. M., and Rasool, S. I. 1974, paper presented at IAU Colloquium 28, Cornell University.
Kliore, A. J., Levy, G. S., Cain, D. L., Fjeldbo, G., and Rasool, S. I. 1967, *Science*, **158**, 1683.
Lewis, J. S. 1971, *Icarus*, **15**, 174.
Matson, D. L., Johnson, T. V., and Fanale, F. P. 1974, *Ap. J. (Letters)*, **192**, L43.
McElroy, M. B., Yung, Y. L., and Brown, R. A. 1974, *Ap. J. (Letters)*, **187**, L127–L130.
Morrison, D., Cruikshank, D. P., and Murphy, R. E. 1972, *Ap. J. (Letters)*, **173**, L143.
Parkinson, T. D. 1974, *J. Atm. Sci.* (in press).
Rapp, D., and Francis, W. E. 1962, *J. Chem. Phys.*, **37**, 2631.
Simpson, J. A., *et al.* 1974, *Science*, **183**, 306.
Sinton, W. M. 1973, *Icarus*, **20**, 284–296.
Smith, B. A., and Smith, S. A. 1973, *Icarus*, **17**, 218.
Trafton, L., Parkinson, T., and Macy, W., Jr. 1974, *Ap. J. (Letters)*, **190**, L85.
Trainor, J. H., Teegarden, B. J., Stilwell, D. E., McDonald, F. B., Roelof, E. C., and Webber, W. R. 1974, *Science*, **183**, 311.
Van Allen, J. A., Baker, D. N., Randall, B. A., Thomsen, M. F., Sentman, D. D., and Flindt, H. R. 1974, *Science*, **183**, 309.

MICHAEL B. McELROY and YUK LING YUNG: Center for Earth and Planetary Physics, Harvard University, Pierce Hall, Cambridge, MA 02138